Hindawi
Geofluids
Volume 2022, Article ID 1895836, 18 pages
https://doi.org/10.1155/2022/1895836

Research Article

Ultra-High-Pressure Hydraulic Slitting Pressure Relief and Penetration Enhancement Technology and Equipment for Soft Coal Seams

Xingang Niu,[1,2,3,4] **Yi Zhao**,[3,4] **Ke Li**,[5] **and Yongjiang Zhang**[3,4]

[1]*State Key Laboratory of Mining Response and Disaster Prevention and Control in Deep Coal Mines, Anhui University of Science and Technology, Huainan, Anhui 232001, China*
[2]*School of Safety Science and Engineering, Anhui University of Science and Technology, Huainan, Anhui 232001, China*
[3]*State Key Laboratory of the Gas Disaster Detecting Preventing and Emergency Controlling, China Coal Technology and Engineering Group Chongqing Research Institute, Chongqing 400037, China*
[4]*Gas Research Branch, China Coal Technology and Engineering Group Chongqing Research Institute, Chongqing 400037, China*
[5]*State Key Laboratory of Coal Mine Disaster Dynamics and Control, School of Resources and Safety Engineering, Chongqing University, Chongqing 400044, China*

Correspondence should be addressed to Xingang Niu; xingang202012@163.com and Ke Li; michealliker@163.com

Received 2 February 2022; Accepted 11 May 2022; Published 16 July 2022

Academic Editor: Basim Abu-Jdayil

There is a "bottleneck effect" in the extraction process of ordinary boreholes. It is crucial to enhance the permeability of the boreholes. In this paper, a set of ultra-high-pressure water jet-based drilling and slotting integrated equipment was designed and applied, and the ultra-high-pressure safeguarding technology of several key components has been studied. Finally, the gas drainage effect of slotted boreholes and ordinary boreholes was investigated through field tests. The test results showed that after using ultra-high-pressure hydraulic slotting, the average drainage concentration of slotted boreholes is 1.49 times that of the ordinary boreholes. The average extraction scalar volume of slotted drilling is 3.02 times that of ordinary boreholes. Under the condition of original content of 12 m^3/t, the extraction radii of slotted boreholes in 3 months and 6 months are 3.76 m and 4.76 m, respectively. The effective radius of the slotted boreholes is 1.76 times that of the ordinary boreholes, which indicate that the ultra-high-pressure hydraulic slotting technology can effectively relieve the pressure and increase the permeability of the soft coal seam.

1. Introduction

China is one of the countries with the most serious coal and gas disasters in the world. With the continuous increase of mining depth and intensity, the characteristics of high gas, high in situ stress, and low permeability are becoming more and more obvious [1–4]. The dangers of in situ stress and gas also increase, the permeability of coal seam decreases, and it becomes more and more difficult to prepump coal seam gas under the condition of unprotected mining [5, 6]. In recent years, the phenomenon of coal and gas dynamic disasters in some deep wells in my country has tended to be complex, with ambiguous characteristics and common disasters. It cannot be explained by the traditional theory of coal and gas outburst, and the existing gas prevention technology and equipment cannot fully meet the needs of coal-rock gas dynamic disaster control in deep mines. For example, the outburst mines in Pingdingshan, Fushun, Fengcheng, Hancheng, and Yaojie mining areas all have common gas disasters in the process of deep mine mining. The detailed rules for gas outburst provide reference to the abnormal coal and gas dynamic phenomena of critical values. The predicted indicators before the disaster did not exceed the standard, but the amount of gas gushing per ton of coal after the disaster was greater than 30 m^3/t. In some mines, such as Xiayukou and Pingdingshan No. 4

and No. 12 mines in Hancheng, Shaanxi Province, obvious in situ stress-dominated gas dynamic disasters occurred during the mining process after the coal seam gas extraction reached the standard. The disaster mechanism of coal-rock gas disasters in deep mines is more complex. Only relying on coal seam gas extraction to meet the standards cannot completely solve the complex disasters of coal-rock layers. Dynamic disaster prevention and control must be carried out from the perspective of coal seam gas extraction standards and effective pressure relief.

In recent years, with the development of high-pressure water jet technology, the method of using high-pressure water to cut coal in the constructed boreholes has achieved certain results, increasing the effect of borehole drainage. There are obvious deficiencies in the slag problem. The quality of the slag discharge directly affects the length of the hole, the extraction efficiency, and the popularization and application of the process. At present, the hydraulic punching pressure is generally 3 MPa~20 MPa, the high-pressure hydraulic cutting pressure is 30 MPa~60 MPa, the radius after low pressure reaming is 200 mm~400 mm, and the high-pressure hydraulic cutting depth is about 500 mm~800 mm. The measures taken for the same hole are relatively simple, and the drill pipe needs to be withdrawn after the drilling construction is completed, and then, the hole reaming and slitting can be performed. There are limitations in the permeability enhancement effect and construction efficiency of low-permeability coal seams, which affect the popularization and application of complete sets of technologies.

Water jet slotting technology has been widely and effectively applied in low-permeability coal mines in my country. At present, the rock breaking theory of water jet mainly includes the static elastic theory [7], stress wave breaking theory [8], and crack propagation breaking theory [9, 10]. However, the relationship between rock failure and failure criteria has not yet been determined, and there is no mature theory to define and describe the water jet failure process of gas-bearing coal in detail. Kong et al. [11, 12] studied the strain characteristics and energy consumption law of gas-bearing coal during shock fracture under jet shock, and the shock failure is closely related to jet pressure. Significant progress has also been made in the research of ultra-high-pressure water jet technology [13]. Various jet cutting technologies such as pulse jet, abrasive jet, and cavitation jet technology have also begun to be applied to the prevention and control of high gas and low permeability coal seams and gas outbursts [14, 15]. At the same time, the research of Lu et al. [16, 17] showed that water jet slitting can release the energy inside the coal seam, reduce the stress of the coal seam, and increase the fracture space in the coal seam. In order to maximize the effect of hydraulic slitting, relevant scholars have conducted a lot of research on the selection of hydraulic slitting process parameters. Yi et al. studied the effect of plugging depth on the gas drainage effect [18]. Zhao et al. analyzed the influence of combination forms of intact sublayer and tectonically deformed sublayer of coal on the gas drainage performance of boreholes [19]. Guo et al. described the mechanism of hole accumulation blasting and antireflection [20]. Hongyu [21] studied the establishment and analysis and evaluation process of the three-dimensional model and analyzed the specific influence of the casing strength by the hydraulic cutting. Houxue [22] used high-pressure hydraulic slitting and antireflection technology to improve the water injection effect of low-permeability coal seams. Huang et al. [23] used high-pressure water jet slotted drilling to improve the gas drainage effect, compared with ordinary drilling to improve gas drainage, and designed a blowout prevention hole device to reduce the gas concentration in the roadway. Tang et al. [24] analyzed that the effect of pressure relief and permeability enhancement of coal seam was affected by the arrangement of hydraulic slits, calculated the lateral depth of the cut coal body, and constructed a three-dimensional finite element model of the hydraulic slits. Zhang et al. [25] analyzed the construction technology of hydraulic kerfs and pointed out the mechanism of hydraulic kerfs; that is, the coal body forms grooves in the kerfs, which leads to the release of gas and in situ stress in the coal seam. Zou et al. [26, 27] analyzed gas flow law in hydraulically slotted coal by setting different slot inclination and pore-to-slot ratio. The above studies have demonstrated the feasibility of the ultra-high-pressure water jet slotted pressure relief and antireflection process from multiple perspectives, but no available equipment and technology have been formed, and there is a lack of field application.

The ultra-high-pressure hydraulic slitting pressure relief and permeability enhancement technology use water as the medium to scour and strip the coal body around the borehole, increase the cracks in the coal body, and greatly improve the gas flow state in the coal seam [28–30]. It creates favorable conditions for gas emission, changes the original stress and fissure condition of the coal body, eases the stress tension in the coal body and surrounding rock, greatly changes the physical and mechanical properties of the coal seam, relieves pressure, and improves permeability and gas permeability. The ability to release gas increases the rate of gas extraction, saves the time required for gas extraction to reach the standard, and effectively relieves the tension of mining replacement. It is one of the development directions of coal mine gas disaster prevention and control measures [31].

2. Ultra-High-Pressure Water Jet Slotted Antireflection Mechanism

2.1. Coal Stress Distribution around the Borehole. Assuming that the surrounding rock is homogeneous and isotropic, the in situ stresses in the vertical and horizontal directions are equal, the cross-section of the borehole is circular, and the borehole is infinitely long; the stress distribution around the borehole is a plane strain problem. The stress and strain of the element are shown in Figure 1.

From the stress balance, we can get

$$(\sigma_r + d\sigma_r)(r + dr)d\theta - \sigma_r r d\theta - 2\sigma_t dr \sin\frac{d\theta}{2} = 0. \quad (1)$$

Ignoring high-order small quantities and using approximate substitution for the sine function, it can be obtained

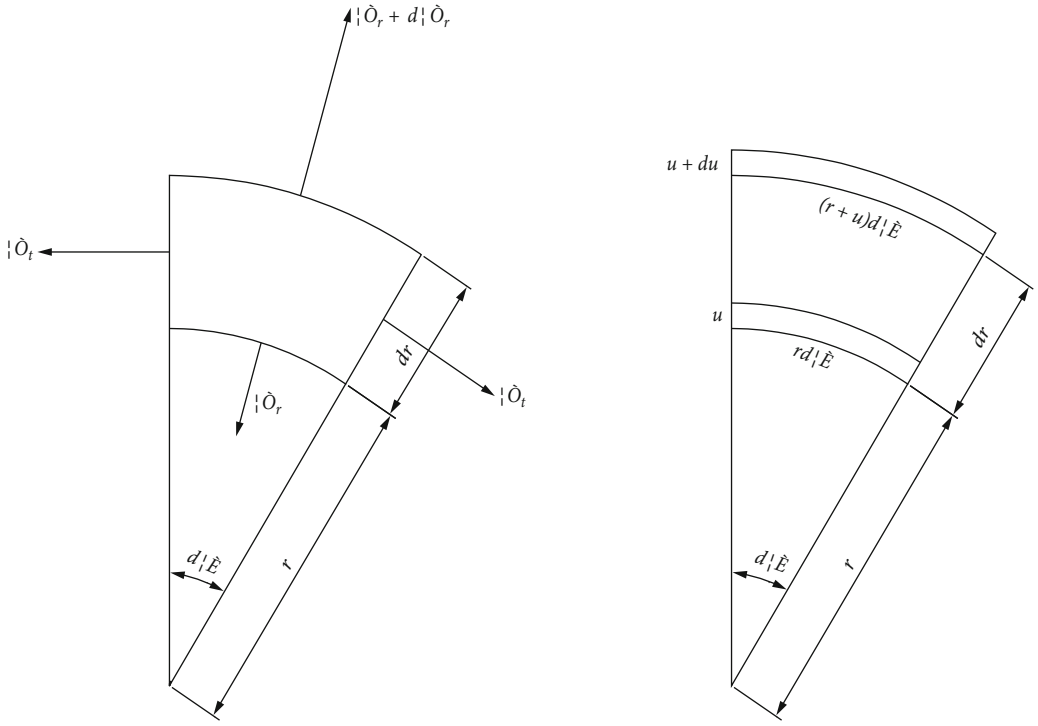

Figure 1: Schematic diagram of force and deformation of surrounding rock unit.

from the generalized Hooke's law; the surrounding rock stress distribution around the borehole is

$$\sigma_r = \gamma H\left(1 - \frac{R^2}{r^2}\right), \tag{2}$$

$$\sigma_t = \gamma H\left(1 + \frac{R^2}{r^2}\right). \tag{3}$$

After the borehole is excavated, the stress is redistributed, and the stress distribution of the surrounding rock is shown in Figure 2. It can be seen from formula (3) that stress concentration occurs around the borehole, and the maximum circumferential stress can reach twice the original in situ stress. After excavation, the fissures around the borehole are closed, and the "bottleneck effect" is prone to occur during the extraction process, which restricts the extraction effect.

The theoretical derivation shows that there is a "bottleneck effect" around the borehole and demonstrates the necessity of ultra-high-pressure hydraulic slitting technology.

2.2. Ultra-High-Pressure Hydraulic Slotting Pressure Relief Mechanism. After the construction of the ordinary drainage hole, due to the small diameter of the hole, the exposed area of coal in the hole is small, and the development of cracks around the hole is not obvious, as shown in Figure 3(a); the influence range of pressure relief is small, and the gas flow in the hole is as follows. In the radial flow as shown in Figure 4(a), there is a "bottleneck effect" in the extraction process. In order to increase the range of extraction and pressure relief and achieve the purpose of rapid and uniform

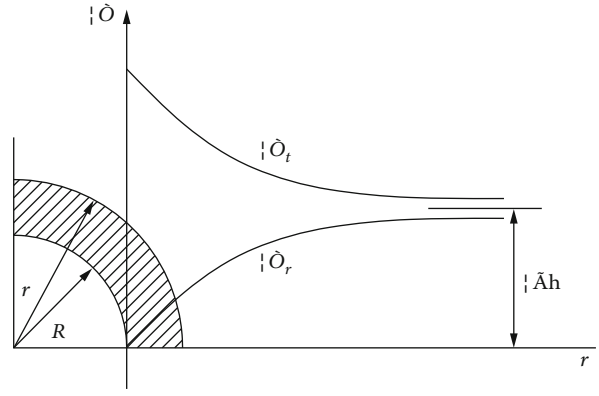

Figure 2: Schematic diagram of stress distribution in surrounding rock of borehole.

pressure relief, it is realized by constructing large-diameter drilling holes or constructing dense drilling holes as shown in Figure 5(a). The amount of drilling engineering is large, and the construction cost is high.

Ultra-high-pressure hydraulic slitting is to use the water hammer pressure and stagnation pressure of ultra-high-pressure water jet to cut the coal body in the borehole after the drilling construction, forming a flat slot with a certain width and depth. The exposed area of the coal body is increased as shown in Figure 3(b), and on the other hand, the deformation space of the coal rock is provided. Since the cutting slot provides the deformation space of coal and rock, the coal body will not undergo elastic-plastic deformation due to the pressure after the in situ stress is loaded

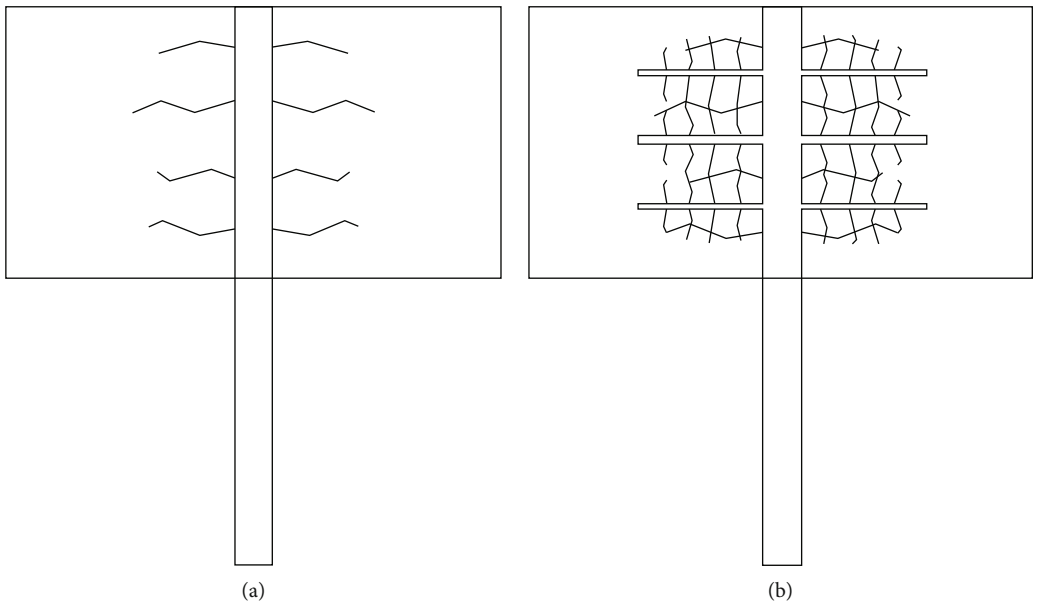

Figure 3: Fissure distribution. (a) Schematic diagram of the development of fissures around ordinary boreholes. (b) Schematic diagram of the development of fissures around the slotted hole.

again. Fissures are shown in Figure 4(b). Macroscopic slits and a large number of secondary fractures together constitute the flow path of analytical gas. The distance between the slits is reasonably controlled, and the combined action of radial flow and interlayer flow between the slits realizes the self-relief of annular network flow between boreholes as shown in Figure 5(b); the pressure relief of the coal body is uniform and sufficient, the overall permeability coefficient of the coal body can be greatly improved, the scope of influence of the extraction is enlarged, and the extraction effect is significantly improved.

3. Ultra-High-Pressure Hydraulic Slitting Equipment Integration and Process Technology

3.1. Ultra-High-Pressure Hydraulic Slitting Complete Equipment Integration. The ultra-high-pressure hydraulic slitting process system is shown in Figure 6.

Quanle et al. [32] studied the drilling-slot-isolation-sealing integrated new technology for improving coalbed methane recovery in underground coal mines, and this paper improves it on the basis. Ultra-high-pressure hydraulic slitting, drilling, and cutting integrated equipment mainly includes diamond composite drill bits, high and low pressure conversion slitters, hydraulic slitting shallow spiral integral drill pipes, ultra-high-pressure rotating water tails, ultra-high-pressure hoses, ultra-high-pressure clean water pumps, high-pressure remote operation console, etc.; the equipment composition is shown in Figure 7.

Compared with ordinary equipment, the ultra-high-pressure hydraulic slitting, drilling, and cutting integrated equipment displayed in this paper is more integrated, and the equipment is more stable and safety.

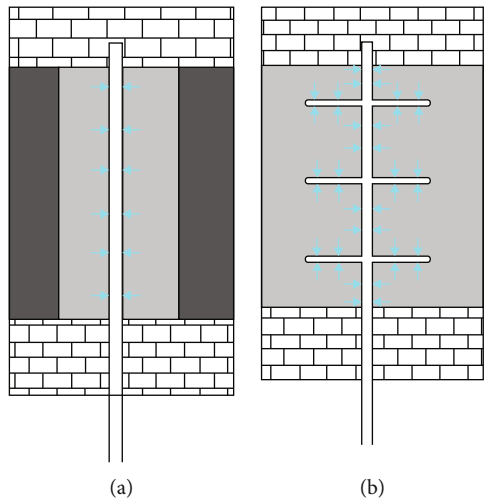

Figure 4: Gas flow around one borehole. (a) Schematic diagram of gas flow in ordinary boreholes. (b) Schematic diagram of gas flow in slotted drilling.

3.1.1. Three-Wing Reinforced Diamond Compact Drill Bit. As shown in Figure 8, the drill bit breaks rock formations according to the principle of scraping and shearing and is suitable for drilling in soft to medium hard formations. It has the characteristics of high wear resistance and high impact resistance, long service life, and high aging and has better advantages in overcoming incomplete formation drilling. The diameter of the drill is generally 113 mm.

3.1.2. High- and Low-Pressure Conversion Slitter. As shown in Figure 9, the slitter can realize the slitting function of coal seam. Realize the free switch between high pressure and low pressure, the low pressure state (pressure lower than 15 MPa) to drill the hole normally, and the high-pressure

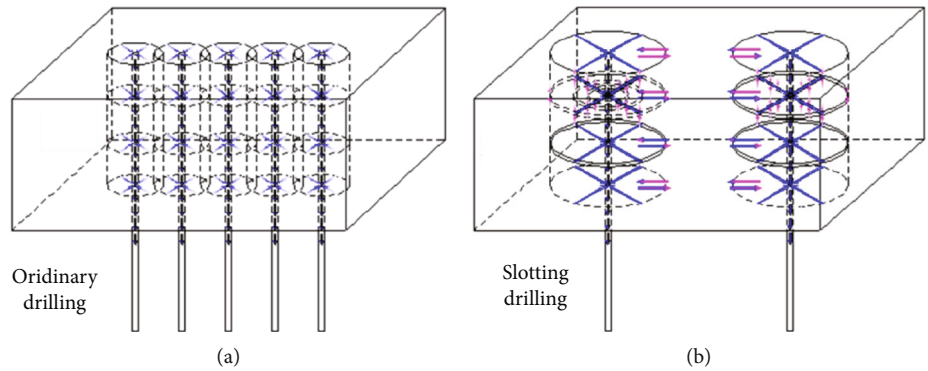

Figure 5: Gas flow around several boreholes. (a) Schematic diagram of extraction of common borehole group. (b) Schematic diagram of drainage of slotted drilling group.

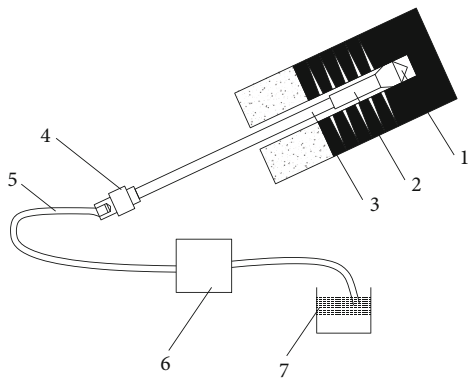

Figure 6: Process system diagram of ultra-high-pressure hydraulic slitting device.

state (pressure greater than 15 MPa); the high and low pressure conversion slitter front end is blocked, and the water is injected from the radial nozzle to form a jet and to slit the coal body. The high and low pressure conversion slitter can withstand the water pressure which is required. For the nozzles of the radial Φ2.5 mm series, the lower limit of the nozzle diameter is determined by formula (4), and the ultra-high-pressure clean water pump is selected with a rated pressure of 100 MPa, a rated flow of 125 L/min, and a power of 250 kW. In the case of a certain output power, the upper limit of the nozzle diameter is determined by formula (5).

$$d \geq \sqrt{u_w\left(D_1^2 - D_2^2\right)\left(\frac{\rho_w}{2P}\right)^{1/2}}, \tag{4}$$

$$d \leq \sqrt{\frac{4Q_e}{\pi}\left(\frac{\rho_w}{2P}\right)^{1/2}}. \tag{5}$$

3.1.3. Hydraulic Slotted Shallow Spiral Integral Drill Pipe. As shown in Figure 10, the drill pipe has the functions of torque output, high-pressure water transportation, and slag discharge in the process of ultra-high-pressure kerfing. It adopts O-ring extrusion seal, three-sealing method, and rough milling groove processing technology on the basis of smooth drill pipe, and the bearing torque is greater than 7200 N·m. The compression ratio and elongation ratio of the O-ring are determined by formula (6) and formula (7) to ensure the sealing performance under the ultra-high-pressure state (pressure above 120 MPa).

$$W = \frac{d_0 - h}{d_0}, \tag{6}$$

$$W = \frac{d + d_0}{d_0 + d_1}. \tag{7}$$

3.1.4. Ultra-High-Pressure Rotating Water Tail. As shown in Figure 11, the water tail is the main channel of high-pressure water transmission. It adopts heavy-duty stainless steel structure and adopts gap seal design. The gap seal is realized by the inner and outer sleeves. The outer diameter of the inner sleeve is slightly smaller than the inner diameter of the outer sleeve. At this time, the gap between the sleeves does not generate water tail rotation resistance and can realize the sealing of water tail through gap throttling. The ultra-high-pressure rotating water tail requires small torque and strong dynamic sealing performance, which can ensure the sensitivity and tightness of rotation under ultra-high-pressure (pressure greater than 100 MPa). The gap width is determined by

$$h = \left(\frac{12\mu_p Lq}{\pi D\Delta p}\right)^{1/3}. \tag{8}$$

3.1.5. Ultra-High-Pressure Hose. As shown in Figure 12, the hose is used for hydraulic transmission and has the characteristics of small fluid resistance, small volume expansion, good chemical corrosion resistance, light weight, and small outer diameter. The ultra-high-pressure hose joint is made of high-quality stainless steel and adopts advanced crimping equipment and technology. The working pressure can reach more than 150 MPa, and the minimum burst pressure can reach 400 MPa. The inner tube is composed of an inner rubber layer, a reinforcing layer, and an outer rubber layer, wherein the reinforcing layer is 6 layers of steel wire

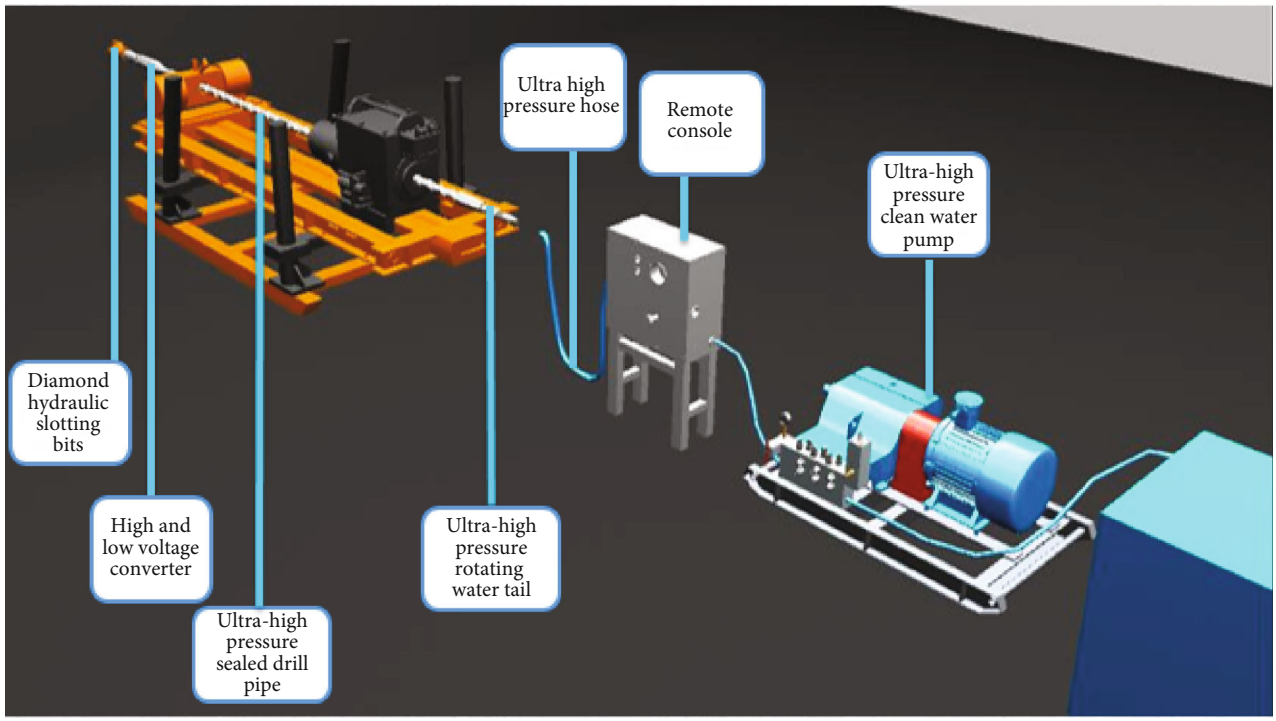

Figure 7: Composition of integrated equipment for ultra-high-pressure hydraulic slitting, drilling, and cutting.

Figure 8: Schematic diagram of diamond compact drill bit.

Figure 9: Schematic diagram of high and low voltage conversion slitter.

winding. The resistance loss along the way during high-pressure water transmission is determined by

$$P = \frac{\mathrm{NLTF}}{2.23D^2}, \tag{9}$$

$$\Delta P = \frac{59.7q^2}{D^5\ \mathrm{Re}^{0.25}}. \tag{10}$$

3.1.6. Ultra-High-Pressure Clean Water Pump. As shown in Figure 13, the water pump is a high-pressure water generating device. The advantages of choosing a horizontal plunger pump are that the pump has a low center of gravity, stable operation, a width of about 1 m, a small volume, and a strong adaptability to the conditions of underground tunnel condition. The rated pressure of the water pump should be greater than the pressure value determined in formula (11) to achieve the depth of the slit.

$$P_p = 0.154sh(|\tau| - c)(b_0 \tan\varphi)^{-1}\left\{1 - D_0 - C_1\left[\frac{(|\tau| - c)(1 - D_0)}{E\tan\varphi}\right]^{\beta}\right\}. \tag{11}$$

The rated flow should be greater than the flow value determined for normal slag discharge in

$$Q = \frac{1}{4}u_w\pi\left(D_1^2 - D_2^2\right). \tag{12}$$

According to the working conditions of the ultra-high-pressure hydraulic slitting device and taking into account the complexity of the underground conditions of the coal mine, the main technical parameters for selecting the high-pressure pump are determined as rated pressure of 100 MPa, rated flow of 125 L/min, and motor power of 250 kW.

Figure 10: Schematic diagram of hydraulic slotted shallow helix integral drill pipe.

Figure 11: Schematic diagram of ultra-high-pressure rotating water tail.

Figure 12: Schematic diagram of ultra-high-pressure hose.

Figure 13: Schematic diagram of ultra-high-pressure clean water pump.

3.1.7. High Voltage Remote Console. As shown in Figure 14, the high-pressure operating table is used for remote control of ultra-high-pressure hydraulic kerfing operations when the pump position is fixed. It is mainly composed of shell, explosion-proof control switch, overflow valve, and pressure gauge. The diameter of the liquid inlet is determined by the rated flow rate and the allowable flow rate, which is determined by

$$d = \sqrt{\frac{4Q_g}{\pi v}}. \tag{13}$$

The design of the main spool is completed by the empirical formula. The diameter of the main spool, the diameter of the piston of the main spool, and the matching length of the main spool and the valve sleeve are calculated by

$$d_1 = (0.5 \sim 0.82)d, \tag{14}$$

Figure 14: Schematic diagram of high-voltage remote console.

Figure 15: Anti-off-chain.

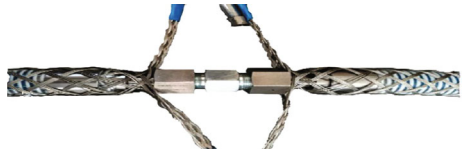

Figure 16: Use diagram of ultra-high-pressure hose and antistripping chain.

$$D_0 = (1.6 \sim 2.3)d_1, \tag{15}$$

$$L = (0.6 \sim 1.5)D_0. \tag{16}$$

The orifice diameter d_0 is selected empirically, and the orifice length is determined by

$$l_0 = (7 \sim 19)d_0. \tag{17}$$

The pilot valve half cone angle is selected empirically, and the valve seat aperture is determined by

$$d_2 = (2 \sim 5)d_0. \tag{18}$$

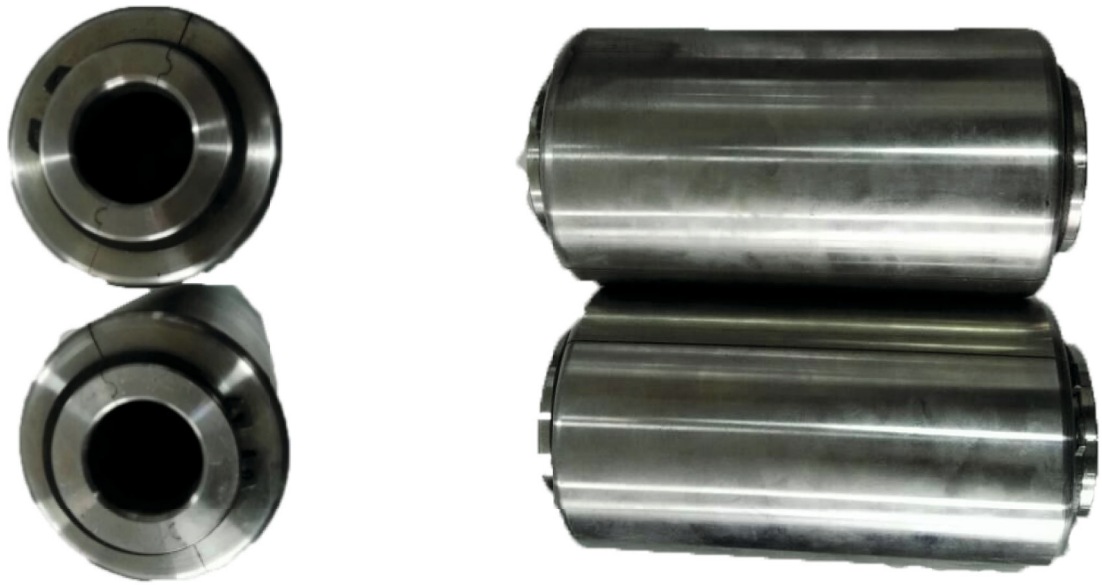

Figure 17: Ultra-high-pressure hose fitting guard.

3.2. Ultra-High-Pressure Safety Technology. In order to ensure the safety of ultrahigh hydraulic transmission, the principle of ultra-high-pressure clean water pump, the performance parameters of transmission equipment, and the selection of protective devices are analyzed.

3.2.1. Ultra-High-Pressure Clean Water Pump. The clean water pump is based on the principle of overflow valve. The nozzle diameter of the configured high and low pressure conversion slitter is 2.5 mm, which can meet the water pressure adjustment of the high-pressure pump to 100 MPa. When the hydraulic transmission equipment is not tightly sealed, damaged, or leaked, it is equivalent to increasing the large diameter of the water outlet prevents the water pressure in the entire system from reaching a high-pressure state.

Equipped with a safety valve, the threshold value of the safety valve is between 105 and 110 MPa, and the maximum working pressure of the ultra-high-pressure hydraulic slitting operation is 100 MPa. When it is opened, the pressure of the entire high-pressure pipeline quickly returns to zero, which effectively ensures the safety of the slitting operation. After closing the ultra-high-pressure clean water pump and then reopening it, the internal valve core of the safety valve can be automatically reset and can continue to be used normally.

3.2.2. Ultra-High-Pressure Hose. Six layers of steel wire winding, the normal working pressure can reach more than 150 MPa, and the minimum burst pressure is 400 MPa. In order to prevent the hoses from falling off, an antidisconnection chain is installed at the end of the hose for secondary protection (as shown in Figures 15 and 16), which can withstand a tensile force of 200 T.

A hose protective sleeve (as shown in Figure 17) is installed at the hose joint for secondary protection to ensure that the hose joint is not exposed.

3.2.3. Ultra-High-Pressure Rotating Water Tail. The ultra-high-pressure rotating water tail is made of heavy-duty stainless steel, which has strong dynamic sealing performance and small torque required for rotation under high pressure, and can withstand high pressure of 140 MPa. The taper hard seal design has strong sealing performance and effectively guarantees the sealing requirements under the working pressure of 100 MPa. In order to prevent water leakage between the ultra-high-pressure rotating water tail and the hose joint during the cutting operation, a water tail sheath (as shown in Figure 18) is installed at the joint for secondary protection, and the joint at the joint is completely wrapped to effectively prevent high-pressure water leaks.

3.2.4. Hydraulic Slotted Shallow Spiral Integral Drill Pipe. Hydraulic slotted shallow spiral integral drill pipe, ultra-high-pressure hose, and ultra-high-pressure rotating water tail are subjected to joint pressure resistance inspection. The inspection pressure reaches 120 MPa, and the pressure is maintained for more than 30 minutes. Combined with the design principle of safety valve and overflow valve of ultra-high-pressure clean water pump, it is equipped with ultra-high-pressure hose joint protective sleeve, antistripping, and ultra-high-pressure rotating water tail sheath for secondary protection, which effectively guarantees the working conditions of 100 MPa cutting seam security. Blowout preventer is installed during the slitting operation to avoid the occurrence of blowhole injury and gas overlimit accident.

4. Field Test Research of Ultra-High-Pressure Water Jet Hydraulic Slotting

4.1. Ultra-High-Pressure Hydraulic Slitting Construction Process. The ultra-high-pressure hydraulic slitting mainly

Figure 18: Ultra-high-pressure rotating water tail jacket.

includes three stages: preparation before slitting, drilling construction, and slitting operation, as shown in Figure 19.

The ultra-high-pressure hydraulic slotting work process is more complicated than the ordinary hydraulic slotting work process, adding ultra-high-pressure equipment and paying more attention to operational safety.

4.2. Ultra-High-Pressure Hydraulic Slitting Test Scheme. The ultra-high-pressure hydraulic slitting test site is selected in the north return air lane. The north return air lane is located in the second panel area of Zhaozhuang Coal Industry. The slitting pressure is set to 100 MPa. The 3# coal seam is the main mining seam, the original gas pressure of the second panel area of the 3# coal seam is 0.594 MPa, the original gas content is 7.90~11.80 m^3/t, the firmness coefficient f is about 0.5, and the permeability coefficient of 3# coal seam is 0.4635~1.7474 MPa^2·d. The initial gas emission of the 100-meter borehole is 0.0052~0.0105 m^3/min·hm, and the gas flow attenuation coefficient of the 100-meter borehole is 0.143~0.29 d^{-1}. The mine's ordinary through-layer drilling is designed according to the drainage radius of 3.8 m, and the column spacing is calculated as 3.5 m. In order to ensure that there is no blind area covered, the value is actually 3.0 m. The 100-meter through-layer drilling has a scalar volume of 0.024~0.039 m^3/min, and the extraction time is 6 months.

In the south side of the north return air lane, a total of 13 rows are designed, and each row is designed with 4 holes (the opening height of the 1# hole in each row is 4 m, the hole height of the 2# hole is 3.5 m, and the hole height of the 3# hole is 3 m and the hole height of the 4# hole is 2.5 m); the first row to the fourth row is the first group, the row spacing is 4 m, the fifth row to the eighth row is the second group, and the row spacing is 5 m; the ninth row to the thirteen rows are the third group. Thirteen rows are the third group, the row spacing is 6 m, the normal spacing between rows is 5 m, and the group spacing is 10 m. The drilling design and construction parameter table are shown in Figure 20 (the drilling holes and row spacing of each group are allowed to be adjusted within 0.2 meters according to the site conditions). Ordinary boreholes, the control group, were arranged in other drilling sites in the same coal seam working face.

4.3. Effect Analysis of Ultra-High-Pressure Hydraulic Slotting Test

4.3.1. Contrastive Analysis of Drainage Effect between Slit and Contrast Hole

(1) Comparative Analysis of Drilling Concentration. Figure 21 shows the average concentration of drilling in the north return wind hydraulic slotted drilling and 2319-2#

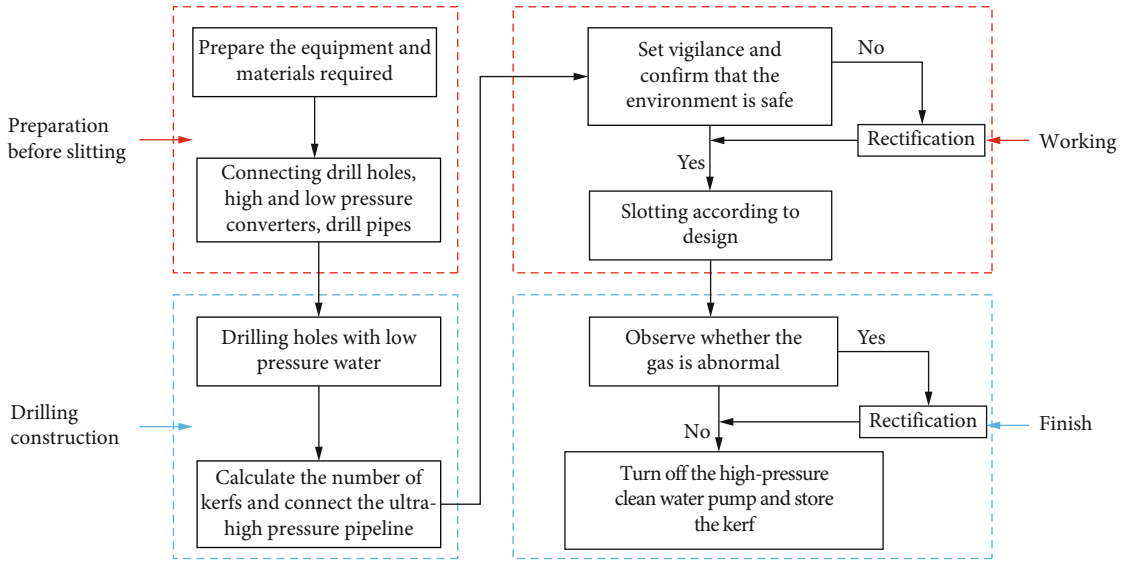

Figure 19: Flow chart of ultra-high-pressure hydraulic kerf operation.

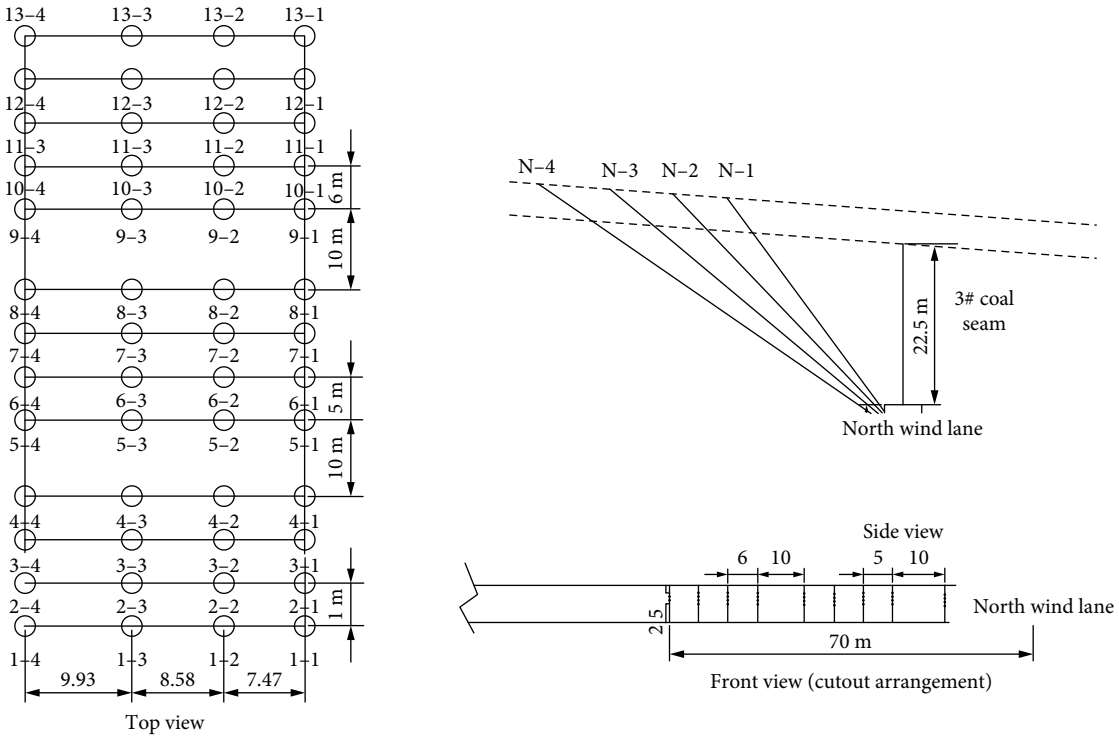

Figure 20: Drilling plan.

bottom pumping roadway in the period of 7 months. It can be seen from the figure that the slotted drilling is from August 19, 2018, to September 9, 2018; during the first stage of cutting, the average concentration of drilling holes was between 27.7 and 37.8%, and the average concentration was 33.0%. During the cutting period, the holes were not sealed in time. Drainage concentration decreased. After all the kerf holes were sealed and pumped around October 9, 2018, the concentration of kerf boreholes rose rapidly. From October 9, 2018, to March 19, 2019, the average concentration of kerf boreholes was 28.7 ~ 50.3%, with an average of 40.2%. After excluding the reasons for the decrease in the concentration of the drilling holes due to the failure to seal the holes in time, it can be concluded that the average concentration of the drilling holes during the extraction time is 33.0%. Also from Figure 21, it can be concluded that the average concentration of the comparative boreholes during the extraction time is between 14.8 and 32.2%, with an average of 22.2%. It can be concluded that

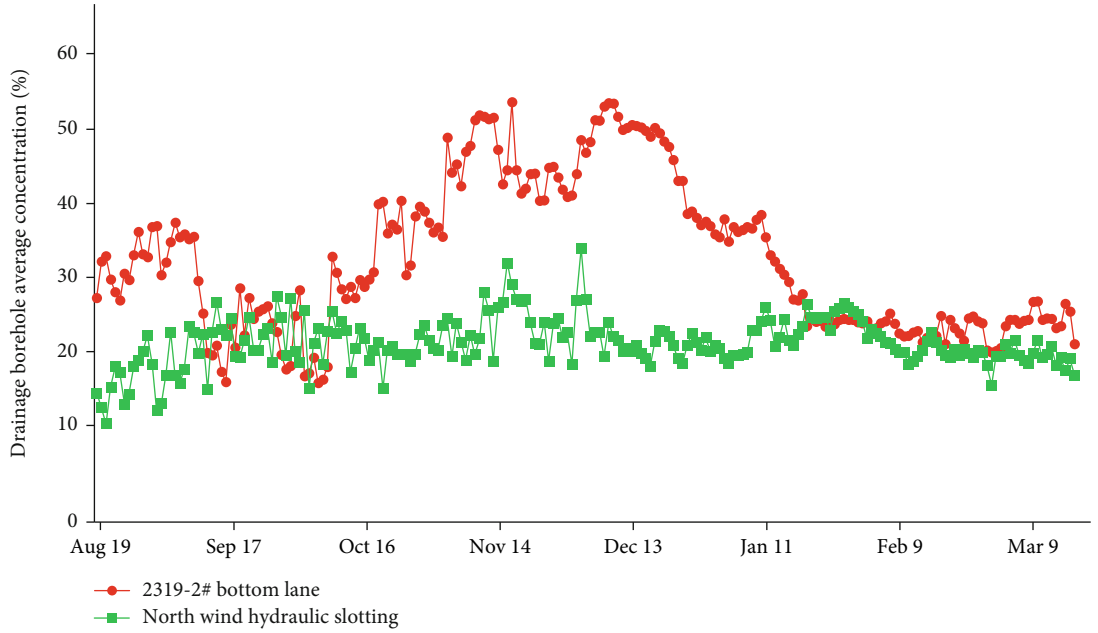

Figure 21: The variation curve of the extraction concentration of the slotted hole and the contrast hole.

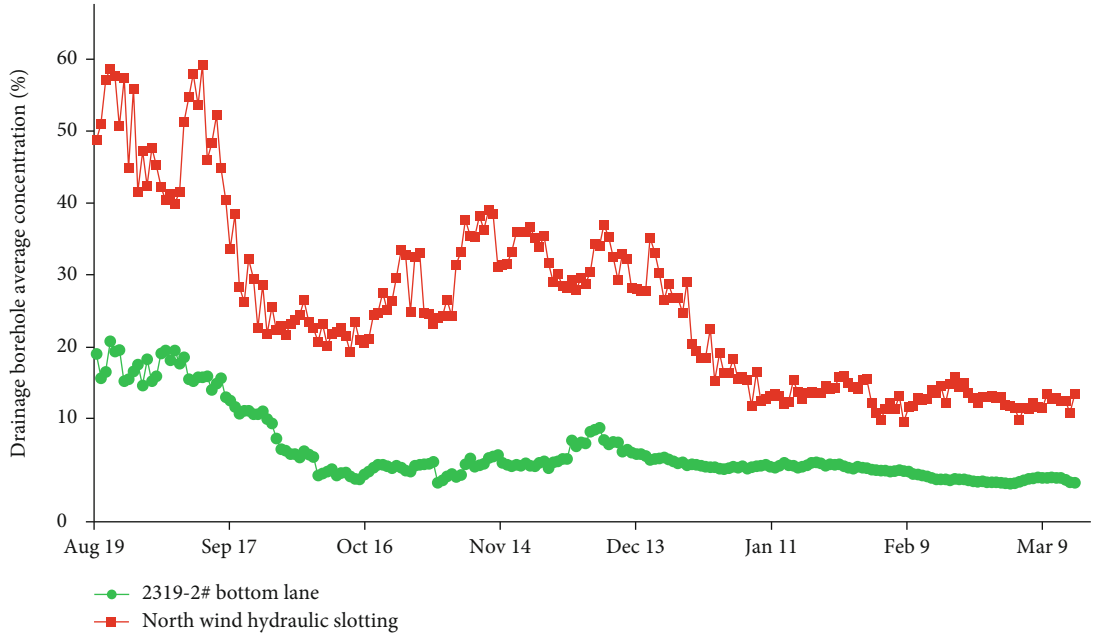

Figure 22: Variation curve of average 100-meter extraction scalar volume between slotted boreholes and comparative boreholes.

the average drainage concentration of the slotted hole is 1.49 times that of the control hole.

(2) Comparison and Analysis of the Scalar Volume of Verabar Monitoring Data Extraction. Figure 22 shows the average extraction scalar data of the 100-meter hole in the extraction time between the slotted hole and the 2319-2# bottom extraction tunnel.

As can be seen from Figure 22, due to the sharp increase in the exposed area of coal in the drilled hole after the slitting, the average 100-meter drilling volume of the slitted hole in the initial period of slitting is relatively large. From August 19, 2018, to around September 10, 2018, the average 100-meter extraction pure volume of slotted drilling was between 0.510 and 0.260 m^3/min, with an average of 0.337 m^3/min. After that, the drainage scalar was also reduced due to the failure to seal the holes in time. After all the holes were sealed and pumped, it can be seen from Figure 22 that the average 100-meter drainage scalar of the slotted holes increased significantly. From October 9, 2018 to March 19, 2019, the average 100-meter drilling scalar volume of slotted boreholes was between

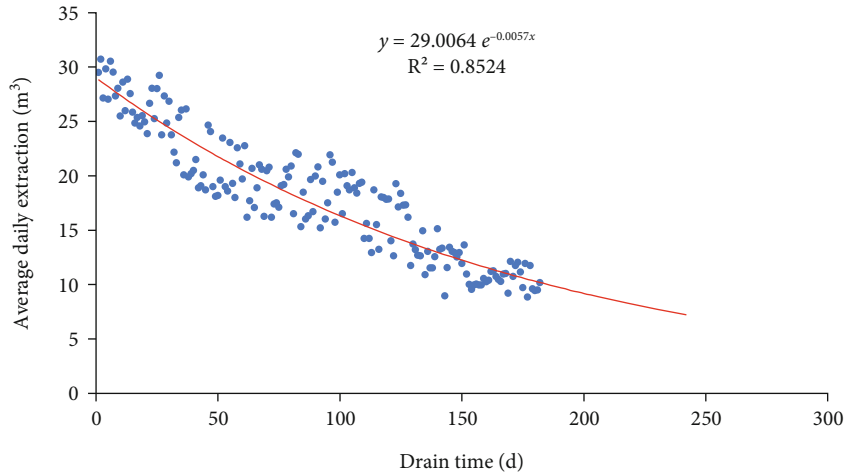

Figure 23: Variation curve of daily average extraction scalar volume with time in slotted boreholes.

0.220 and 0.145 m^3/min, with an average drilling scalar volume of 0.197 m^3/min.

Generally speaking, the average 100-meter drilling purities of comparative drainage drilling are between 0.030 and 0.142 m^3/min, and the average is 0.056 m^3/min. The amount is 0.107~0.510 m^3/min, with an average of 0.169 m^3/min; it can be concluded that the average 100-meter drilling scalar volume of the ultra-high-pressure hydraulic slitting drilling is 3.02 times that of the comparison drilling.

Drainage borehole flow was disturbed by many factors in field tests, but the difference between the curves of slotted boreholes and contrast boreholes was significant.

4.3.2. Comparative Analysis of Drilling Radius

(1) Investigation of Drilling Gas Drainage Law. In order to investigate the effect of borehole predrainage gas, the characteristic parameters that characterize the variation law of borehole gas drainage with time, initial borehole gas drainage (q_{co}) and gas drainage attenuation coefficient (β), were measured. In order to ensure the accuracy and representativeness of the measurement results, the method of grouping according to the drilling distance was adopted. During the measurement, a measurement array (t, q_{ct}) is formed according to the mixed flow rate, mixed concentration, extraction time, and drill hole length of each drilling hole every day, combined with the drilling time (t) for drilling. The values of q_{co} and q can be obtained by the following regression analysis according to the (t, q_{ct}) array.

$$Q_{SC} = Q_{WC}^{P_1 T_0 / P_0 T_1}, \tag{19}$$

where Q_{SC} is the standard state gas flow, m^3/min; Q_{WC} is the gas flow in working condition, m^3/min; P_0 is the standard atmospheric pressure, Pa; P_1 is the absolute pressure of the orifice of the drainage hole, Pa; T is the absolute temperature of the gas from the borehole orifice, K; T_0 is standard state absolute temperature, K; and t is the temperature of the gas at the orifice of the drilling hole, °C.

The gas drainage volume q_{ct} of the borehole and the drainage time t of the borehole are in good agreement with the negative exponential function relationship, as follows:

$$q_{ct} = q_{c0} e^{-\beta t}, \tag{20}$$

where q_{c0} is the initial gas extraction volume of the borehole, m^3/min; q_{ct} is the average gas drainage volume of boreholes at the drainage time t, m^3/min; β is the attenuation coefficient of borehole gas drainage, d^{-1}; and t is the gas extraction time of the borehole, d.

When the implemented gas drainage boreholes are draining, the gas flow field between the boreholes is a finite source gas flow field. As time goes by, the boreholes will affect each other. In this case, a group of gas drainage boreholes with different spacing were constructed in the original coal body, and the gas-related parameters of the middle part of the boreholes that were closest to the gas environment around the on-site drainage boreholes were investigated. Fit the observed gas flow rate and time for each group of boreholes, and the fitting curve is as follows.

The relationship between kerf drilling flow rate and time function is

$$q_{slot} = 29.0064 e^{-0.0057x}. \tag{21}$$

Figure 23 shows the variation curve of slot drilling flow rate with time.

The relationship between the flow rate of ordinary drainage holes and time function is

$$q_s = 9.6091e - 0.0062x. \tag{22}$$

Figure 24 shows the variation curve of ordinary drainage borehole flow rate with time.

It can be seen from the relationship between the gas flow and time of the slotted hole and the ordinary hole: the extraction scalar decreases with the increase of the extraction

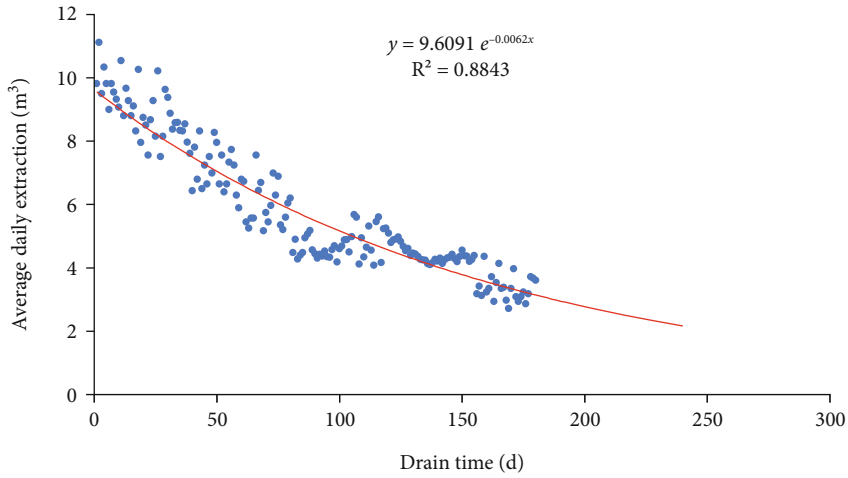

Figure 24: Variation curve of daily average scalar extraction volume with time in common extraction boreholes.

time in a negative exponential relationship. The longer the extraction time, the smaller the gas extraction flow. The smaller the distance between the drilling holes, the greater the attenuation coefficient of gas drainage flow, which means that under the conditions of the same area of coal, the same drainage time, and the same gas content in the original coal seam, the smaller the distance between the drilling holes, the more the gas content decreases after extraction.

Integrating Equation (22), the total amount of borehole gas drainage in any time t day can be obtained Q_{ct}:

$$Q_{ct} = \int_0^t q_{c0} e^{-\beta t} = \frac{q_{c0}\left(1 - e^{-\beta t}\right)}{\beta}, \tag{23}$$

where Q_{ct} is the total amount of borehole gas drainage in time t, m^3, and Q_{cj} is $t \longrightarrow \infty$ drilling limit gas extraction volume, m^3.

According to Equation (23), the relationship between the total gas drainage flow of slotted boreholes and ordinary boreholes and the drainage time is as follows:

The relationship between the total flow rate of kerf drilling and time function is

$$Q_s = 5088.84 \times \left(1 - e^{-0.0057t}\right). \tag{24}$$

The relationship between the total flow of ordinary drainage holes and the time function is

$$Q_c = 1549.85 \times \left(1 - e^{-0.0062t}\right) \tag{25}$$

The relationship between the total gas drainage flow and time of slotted drilling and ordinary drilling can be seen: the total gas drainage flow of the drilling hole increases with the increase of the drainage time in a negative exponential relationship. The total increase and change are getting smaller and smaller. The larger the distance between the drainage holes, the larger the limit value of the total flow rate of drilling gas drainage.

Table 1: Calculation results of kerf drilling radius.

Cumulative extraction days	Single hole (average) cumulative total drainage (m^3)	Number of holes to be drilled (pcs)	Drainage radius (m)
30	880.23	51.04	2.47
60	1352.92	33.21	3.07
90	1943.50	23.12	3.67
120	2559.15	17.56	4.21
150	2963.52	15.16	4.54
180	3256.40	13.80	4.76

(2) Calculation of Effective Radius for Slotting Drilling.

(1) Analysis based on measured data

The gas extraction radius of the slotted borehole in the north return airway to inspect the borehole control area needs to be extracted as

$$\begin{aligned} Q_{DA} &= L_1 \times L_2 \times h \times \gamma \times (W - 8) \\ &= 26 \times 48 \times 6 \times 1.50 \times (12 - 8) = 44928\ m^3. \end{aligned} \tag{26}$$

In the formula, L_1 refers to the length of the control area of the drainage hole, and L_2 refers to the width of the area on both sides of the drainage hole to control the roadway.

The calculation results of the average single-hole cumulative gas drainage scalar and drainage radius under different drainage time of slotted drilling are shown in Table 1.

(2) Calculate the extraction radius according to the fitting curve

According to the daily average scalar gas drainage data of slotted boreholes, the negative exponential curve of drainage attenuation is obtained. As shown in Figure 23, the data correlation is strong, and the negative exponential curve of

attenuation can effectively represent the single drilling volume of slotted boreholes. According to the gas drainage law of hole drainage, the drainage radius of slotted hole can be calculated integrally according to the negative exponential curve formula of drainage attenuation, as shown in Table 2.

$$Q_t = \int_0^t 29.0064e^{-0.0057t}dt = \frac{29.0064}{0.0057} - \frac{29.0064}{0.0057}e^{-0.0057t}. \quad (27)$$

Comparing the above calculation results, the drilling radius calculated by the statistics is basically consistent with the drilling radius calculated by the integral of the negative exponential curve of the drainage attenuation.

(3) Comparing the Effective Radius Calculation of Drilling Hole Extraction.

(1) Analysis based on measured data

2319-2# bottom-draining roadway, compared with the extraction radius of the drilling hole, and the amount of gas that needs to be drained in the control area of the drilling hole is

$$\begin{aligned} Q_{DA} &= L_1 \times L_2 \times h \times \gamma \times (W - 8) \\ &= 138 \times 39 \times 6 \times 1.5 \times (12 - 8) = 193752\ \text{m}^3. \end{aligned} \quad (28)$$

Table 3 shows the average single-hole cumulative gas drainage scalar volume statistics and the calculation results of the drainage radius of the 2319-2# bottom drainage tunnel under different drainage time.

(2) Calculate the extraction radius according to the fitting curve

According to the daily average scalar gas drainage data of the comparison drilling, the negative exponential curve of drainage attenuation is obtained. As shown in Figure 24, the data correlation is strong, and the negative exponential curve of attenuation can effectively represent the single hole drainage of the comparison drilling. According to the gas extraction law, the extraction radius of the drilling hole can be calculated and calculated integrally according to the negative exponential curve formula of extraction attenuation, and the results are shown in Table 4.

$$Q_t = \int_0^t 9.6091e^{-0.0062t}dt = \frac{9.6091}{0.0062} - \frac{9.6091}{0.0062}e^{-0.0062t}. \quad (29)$$

As shown in Figure 25, comparing the above calculation results, the drilling radius calculated by the statistics is basically consistent with the drilling radius calculated by the integral of the negative exponential curve of the drainage attenuation.

Table 2: Calculation results of the extraction radius of the slotted hole (fitting the negative exponential curve of extraction attenuation).

Cumulative extraction days	Single hole cumulative total drainage (m^3)	Number of holes to be drilled (pcs)	Drainage radius (m)
30	797.61	56.33	2.35
60	1470.22	30.56	3.19
90	2037.39	22.05	3.76
120	2515.67	17.86	4.17
150	2918.99	15.39	4.51
180	3259.09	13.79	4.76

Table 3: Comparison of the calculation results of the drilling radius.

Cumulative extraction days	Single hole (average) cumulative total drainage (m^3)	Number of holes to be drilled (pcs)	Drainage radius (m)
30	350.17	553.31	1.56
60	518.30	373.82	1.90
90	645.86	299.99	2.12
120	811.61	238.73	2.37
150	944.08	205.23	2.56
180	1068.96	181.25	2.73

Table 4: Comparison of the calculation results of the extraction radius of the borehole (fitting the negative exponential curve of extraction attenuation).

Cumulative extraction days	Single hole cumulative total drainage (m^3)	Number of holes to be drilled (pcs)	Drainage radius (m)
30	262.32	783.61	1.31
60	480.24	403.45	1.83
90	661.28	293.00	2.14
120	811.67	238.71	2.37
150	936.61	206.87	2.55
180	1040.41	186.23	2.69

Through the above analysis, it can be seen that the drainage radius of the slotted hole is 3.76 m and 4.76 m after 3 months and 6 months of drainage; meanwhile, the drainage radius after 3 months and 6 months of drainage of the comparison hole is respectively 2.14 m and 2.69 m. It can be seen that the effective radius of kerf drilling is 1.76 times that of the comparison drilling.

4.3.3. Residual Gas Content. In order to verify the drainage effect, the residual gas content in the vicinity of the borehole was measured in the slotted borehole and the comparative borehole for 3 months and 6 months, respectively. The result is as follows.

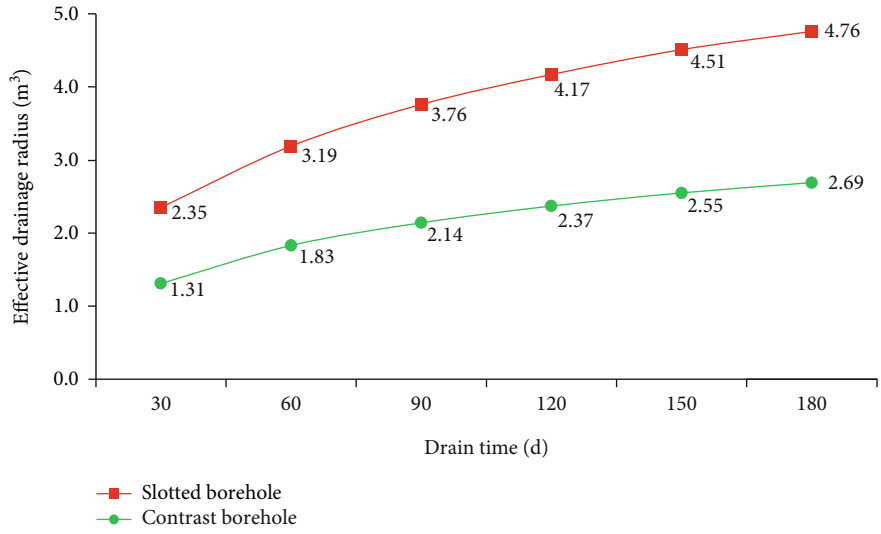

Figure 25: Change curve of effective radius of kerf drilling and comparative drilling.

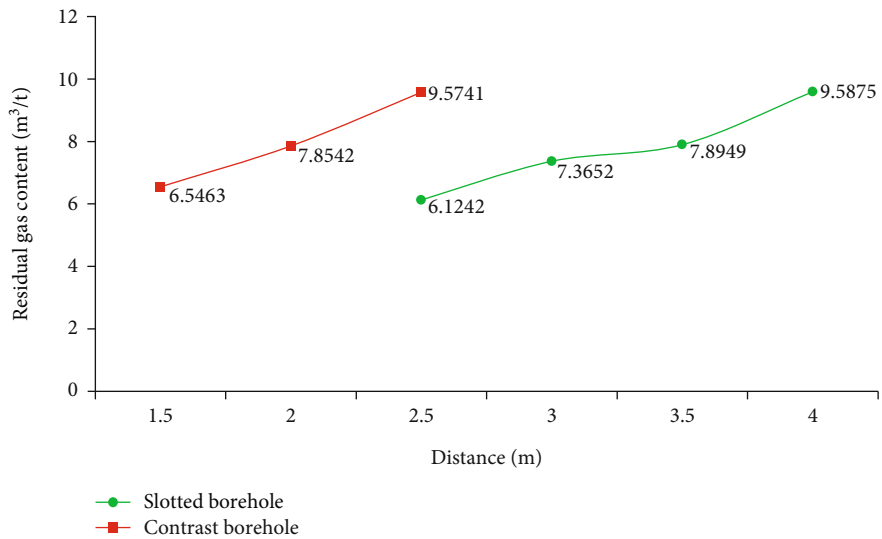

Figure 26: Determination results of residual gas content after 3 months of extraction.

Figure 26 shows the sampling results of the kerf and the vicinity of the comparative borehole after 3 months of extraction. It can be seen from the figure that the residual gas content at the 1.5 m and 2.0 m positions of the comparison hole is less than 8 m^3/t, and the residual gas content at the 2.5 m position is greater than 8 m^3/t, indicating that the comparison hole was drained after 3 months of extraction. The effective radius is between 2.0 m and 2.5 m, which is consistent with the calculation results; the residual gas content at the 2.5 m, 3.0 m, and 3.5 m positions of the slotted hole is less than 8 m^3/t, and the residual gas content at the 4.0 m position is greater than 8 m^3/t, indicating that the effective radius of the slotted hole for drainage is between 3.5 m and 4.0 m after 3 months of extraction, which is consistent with the calculation results.

Figure 27 shows the results of sampling near the kerf and the comparative borehole after 6 months of extraction. It can be seen from the figure that the residual gas content at the 2.0 m and 2.5 m positions of the comparison hole is less than 8 m^3/t, and the residual gas content at the 3.0 m position is greater than 8 m^3/t, indicating that the comparison hole was drained after 3 months of extraction. The effective radius is between 2.5 m and 3.0 m, which is consistent with the calculation results; the residual gas content at the 3.5 m, 4.0 m, and 4.5 m positions of the slotted hole is less than 8 m^3/t, and the residual gas content at the 5.0 m position is greater than 8 m^3/t, indicating that the effective radius of the slotted hole for drainage is between 4.5 m and 5.0 m after 3 months of extraction, which is consistent with the calculation results.

According to the design parameters of drilling holes, the design parameters of slotted drilling holes are the row spacing of 4 m and the normal spacing between drilling rows of 5 m. Therefore, it can be calculated that the total amount

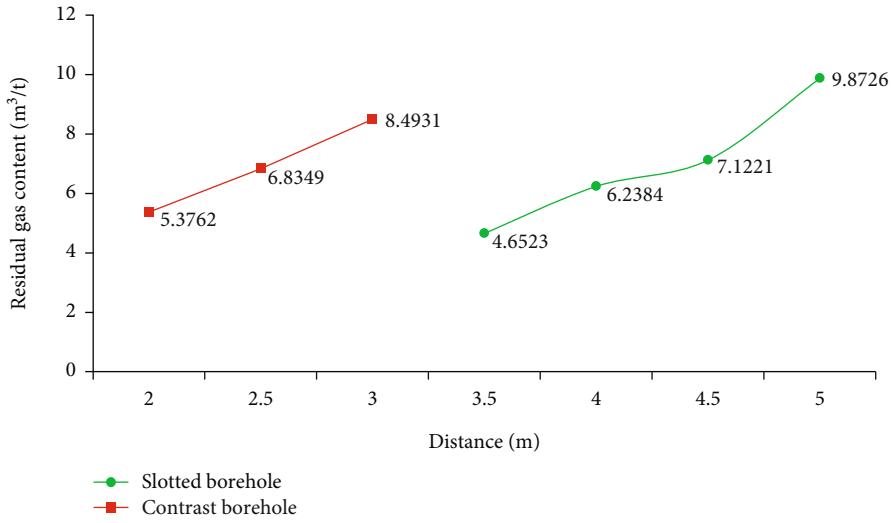

Figure 27: Determination results of residual gas content after 6 months of extraction.

Table 5: Comparison of the amount of work between slotted drilling and comparative drilling.

	Contrast hole	Slotted hole	Contrast value
Drilling arrangement parameters	Row spacing 3 m, normal spacing 4 m	Row spacing 4 m, normal spacing 5 m	46% reduction in drilling work in the same area
Average 100-meter-per-hole extraction scalar volume within 6 months	0.056 m^3/min	0.169 m^3/min	3.02 times
The total amount of gas extraction in the same area has increased	~	~	71.6%
Effective radius of drilling for 6 months of drilling (m)	4.76	2.69	1.76 times

of drilling gas drainage increases by 71.6%, and the effective radius of drainage increases by 76% on the basis of a 46% reduction in drilling engineering volume in the same control area, and the comparison results are shown in Table 5.

5. Conclusions

Through theoretical analysis, field test, and other methods, the ultra-high-pressure hydraulic cutting seam pressure relief and permeability enhancement technology for soft coal seams are studied, and the following conclusions are drawn:

(1) After conventional drilling construction, the "bottleneck effect" is prone to restrict the extraction effect; ultra-high-pressure hydraulic slitting measures are adopted, and the high-pressure water cuts the coal body to form circular slits with equal spacing, macroslits, and secondary fractures. The gas flow path in the slot is changed, the permeability of the coal seam is improved, and the self-pressure relief effect of the drilled mesh slotted slot is used to achieve the goal of rapid and uniform pressure relief and permeability enhancement

(2) For the ultra-high-pressure water jet slotting technology, the ultra-high-pressure hydraulic slotting drilling and cutting integrated equipment is designed, including the diamond composite drill bit, the high-low pressure conversion slotter, the hydraulic slotting shallow spiral integral drill pipe, the ultra-high-pressure rotating water tail, ultra-high-pressure hoses, ultra-high-pressure clean water pumps, high-pressure remote consoles, etc.; and on this basis, for ultra-high-pressure clean water pumps, ultra-high-pressure hoses, ultra-high-pressure rotating water tails, and hydraulic slitting shallow spiral integral drill pipe have been formed and on this basis, a set of ultra-high-pressure safety protection technology has been formed included ultra-high-pressure clean water pumps, ultra-high-pressure hoses, ultra-high-pressure rotating water tails and hydraulic slitting shallow spiral integral drill pipe

(3) The results of the downhole test show that after the ultra-high-pressure hydraulic slitting is used, the average drainage concentration of the slitted hole is 1.49 times that of the ordinary hole. Under the condition of the original content of 12 m^3/t, the drainage radius of the slotted hole is 3.76 m and 4.76 m after 3 months and 6 months of extraction; the effective radius of the slotted hole is 1.76 times that of the control hole

Data Availability

The research data used to support the findings of this study are available from the corresponding author upon request.

Conflicts of Interest

The authors declare that they have no conflicts of interest

Acknowledgments

The authors would like to thank the Technological Innovation and Entrepreneurship Fund Special Project of Tiandi Technology Co., Ltd. (2021-2-TD-ZD008) (Research on Self-Relief Technology and Equipment of Bedding Directional Hydraulic Slitting) and the Open Fund of the State Key Laboratory of Deep Coal Mining Response and Disaster Prevention and Control (SKLMRDPC20KF01) (Prevention and Control Technology of Cross-Cutting, Longitudinal Breaking, Unloading and Energy Dissipation for Coal-Rock Composite Dynamic Disasters in Deep Mines). The authors acknowledge financial support provided by the National Natural Science Foundation of China (52074120).

References

[1] W. Yang, B.-q. Lin, Q. Yong-an et al., "Mechanism of strata deformation under protective seam and its application for relieved methane control," *International Journal of Coal Geology*, vol. 85, no. 3-4, pp. 300–306, 2011.

[2] Q. Zou, L. Han, Z. Yongjiang, F. Li Qingmiao, and J.,. H. Qianting, "Rationality evaluation of production deployment of outburst-prone coal mines: a case study of Nantong Coal Mine in Chongqing, China," *China. Safety Science*, vol. 122, article 104515, 2020.

[3] X. Li, S. Chen, S. Wang, M. Zhao, and H. Liu, "Study on in situ stress distribution law of the deep mine taking Linyi mining area as an example," *Advances in Materials Science and Engineering*, vol. 9, no. 4, Article ID 5594181, 6 pages, 2021.

[4] W. Yang, B.-q. Lin, Q. Yong-an et al., "Stress evolution with time and space during mining of a coal seam," *International Journal of Rock Mechanics and Mining Sciences*, vol. 48, no. 7, pp. 1145–1152, 2011.

[5] Q. Zou, T. Zhang, Z. Cheng, Z. Jiang, and S. Tian, "A method for selection rationality evaluation of the first-mining seam in multi-seam mining," *Geomechanics and Geophysics for Geo-Energy and Geo-Resources*, vol. 8, no. 1, p. 17, 2022.

[6] Q. Zou, T. Zhang, T. Ma, S. Tian, X. Jia, and Z. Jiang, "Effect of water-based SiO_2 nanofluid on surface wettability of raw coal," *Energy*, vol. 254, p. 124228, 2022.

[7] M. Kondo, K. Fujii, and H. Syoji, *On the Destruction of Mortar Specimens by Submerged Water Jets*, Proceedings of the Second International Symposium on Jet Cutting Technology, Cambridge, U.K, 1974.

[8] S. Kang, T. Reitter, and G. Carlson, "Target responses to the impact of high-velocity, non-abrasive water jests," in *Proceedings of the 7th American Water Jet Conference*, Seattle, Washington, 1993.

[9] S. C. Crow, P. V. Lade, and G. H. Hurlburt, "The mechanics of hydraulic rock cutting," *International Journal of Rock Mechanics and Mining Sciences & Geomechanics Abstracts*, vol. 10, 1973.

[10] J. Feng, E. Wang, Q. Huang, H. Ding, and X. Zhang, "Experimental and numerical study of failure behavior and mechanism of coal under dynamic compressive loads," *International Journal of Mining Science and Technology*, vol. 30, no. 5, pp. 613–621, 2020.

[11] X. G. Kong, D. He, X. F. Liu et al., "Strain characteristics and energy dissipation laws of gas-bearing coal during impact fracture process," *Energy*, vol. 242, article 123028, 2022.

[12] X. G. Kong, S. G. Li, E. Y. Wang et al., "Experimental and numerical investigations on dynamic mechanical responses and failure process of gas-bearing coal under impact load," *Soil Dynamics and Earthquake Engineering*, vol. 142, article 106579, 2021.

[13] V. Sharma, S. Chattopadhyaya, and S. Hloch, "Multi response optimization of process parameters based on Taguchi-Fuzzy model for coal cutting by water jet technology," *International Journal of Advanced Manufacturing Technology*, vol. 56, no. 9-12, pp. 1019–1025, 2011.

[14] C. Shen, B. Lin, F. Meng, Q. Zhang, and C. Zhai, "Application of pressure relief and permeability increased by slotting a coal seam with a rotary type cutter working across rock layers," *International Journal of Mining Science and Technology*, vol. 22, no. 4, pp. 533–538, 2012.

[15] T. Shen, Y. B. Wang, D. Z. Tang et al., "Dynamic variation effects of coal permeability during the coalbed methane development process in the Qinshui Basin, China," *International Journal of Coal Geology*, vol. 93, pp. 16–22, 2012.

[16] T. K. Lu, H. Yu, T. Y. Zhou, J. S. Mao, and B. H. Guo, "Improvement of methane drainage in high gassy coal seam using waterjet technique," *International Journal of Coal Geology*, vol. 79, no. 1-2, pp. 40–48, 2009.

[17] T. K. Lu, Z. J. Zhao, and H. F. Hu, "Improving the gate road development rate and reducing outburst occurrences using the waterjet technique in high gas content outburst-prone soft coal seam," *International Journal of Rock Mechanics and Mining Sciences*, vol. 48, no. 8, pp. 1271–1282, 2011.

[18] M. Yi, L. Wang, C. Hao, Q. Liu, and Z. Wang, "Method for designing the optimal sealing depth in methane drainage boreholes to realize efficient drainage," *Int J Coal Sci Technol*, vol. 8, no. 6, pp. 1400–1410, 2021.

[19] W. Zhao, K. Wang, R. Zhang, D. Huzi, Z. Lou, and A. Fenghua, "Influence of combination forms of intact sub-layer and tectonically deformed sub-layer of coal on the gas drainage performance of boreholes: a numerical study," *International Journal of Coal Science & Technology*, vol. 7, no. 3, pp. 571–580, 2020.

[20] D. Guo, P. Lv, J. Zhao, and C. Zhang, "Research progress on permeability improvement mechanisms and technologies of coalbed deep-hole cumulative blasting," *Int J Coal Sci Technol*, vol. 7, no. 2, pp. 329–336, 2020.

[21] W. Hongyu, "Analysis of casing strength after hydraulic slitting and discussion on supporting fracturing technology," *Chemical Engineering and Equipment*, vol. 8, pp. 105–107, 2016.

[22] X. Houxue, "Research on the technology of water injection and dust suppression by slitting along the bedding hole in low permeability coal seams," *Coal Science and Technology*, vol. 9, pp. 29–38, 2016.

[23] C. Huang, Z. Dai, and M. Guo, "Research on high-pressure water jet slot enhanced gas drainage and blowout prevention

technology," *Coal Science and Technology*, vol. 4, pp. 63–66, 2015.

[24] J. Tang, S. Yang, and L. Li, "Numerical simulation of the effect of different hydraulic slit arrangements on pressure relief and outburst prevention," *Chinese Journal of Geological Hazards and Prevention*, vol. 1, pp. 61–66, 2012.

[25] L. Zhang, B. Lin, and Y. Gao, "Rapid outburst elimination technology in coal roadway based on high-pressure hydraulic slitting technology," *Coal Mine Safety*, vol. 3, pp. 64–66, 2013.

[26] Q. Zou, H. Liu, Z. Cheng, T. Zhang, and B. Lin, "Effect of slot inclination angle and borehole-slot ratio on mechanical property of pre-cracked coal: implications for ECBM recovery using hydraulic slotting," *Natural Resources Research*, vol. 29, no. 3, pp. 1705–1729, 2020.

[27] Q. Zou, H. Liu, Z. Jiang, and W. Xueang, "Gas flow laws in coal subjected to hydraulic slotting and a prediction model for its permeability-enhancing effect," *Energy Sources, Part A: Recovery, Utilization, and Environmental Effects*, 2021.

[28] B. Q. Lin, W. Yang, H. J. Wu, F. W. Meng, Y. X. Zhao, and C. Zhai, "A numeric analysis of theeffects different factors have on slotted drilling," *Journal of China University of Mining & Technology*, vol. 39, no. 2, pp. 153–157, 2010.

[29] B. Zhang, Q. He, Z. Lin, and Z. Li, "Experimental study on the flow behaviour of water-sand mixtures in fractured rock specimens," *International Journal of Mining Science and Technology*, vol. 31, no. 3, pp. 377–385, 2021.

[30] G. K. Srivastava and M. S. R. Murthy Vemavarapu, "Drillability prediction in some metamorphic rocks using composite penetration rate index (CPRI) - an approach," *Mining Science and Technology*, vol. 31, no. 4, pp. 631–641, 2021.

[31] X. Li, Z. Cao, and X. Youlin, "Characteristics and trends of coal mine safety development, energy sources," *Part A: Recovery, Utilization, and Environmental Effects*, pp. 1–14, 2020.

[32] Z. Quanle, L. Baiquan, Z. Chunshan et al., "Novel integrated techniques of drilling-slotting-separation-sealing for enhanced coal bed methane recovery in underground coal mines," *Journal of Natural Gas Science and Engineering*, vol. 26, pp. 960–973, 2015.